Baseline for the LhARA design update

The LhARA collaboration

1 Introduction

The LhARA facility has been designed to serve two end stations for *in-vitro* radiobiology and one end station for *in-vivo* studies. The principle components of Stage 1 of the LhARA accelerator are: the laser-driven proton and ion source; the matching and energy-selection section; beam delivery to the low-energy *in-vitro* end station; and the low-energy abort line.

Stage 2 is formed by the injection line for the fixed-field alternating-gradient accelerator (FFA); the FFA; the extraction line; the high-energy abort line; beam delivery to the high-energy *in-vitro* end station; and the transfer line to the *in-vivo* end station. Proton beams with energies of between 10 and 15 MeV will be delivered directly from the laser-driven source to the low-energy *in-vitro* end station via a transfer line. The high energy *in-vitro* end station and the *in-vivo* end station will be served by proton beams with energy between 15 and 127 MeV and by ion beams, including C^{6+} with energies up to 33.4 MeV/u.

The present technical note summarises the most recent design parameters of the facility. Most of the components of LhARA were described in the "pre Conceptual Design Report" (pre-CDR) [1] which laid the foundations for the development of full conceptual and technical design reports for the facility. Some of the parameters have been updated since the publication of the pre-CDR as a result of specific optimisations. For example, the focusing strength of the Gabor lenses and the collimators in the Stage 1 have been optimised to increase the transport efficiency of a proton beam obtained from 2-D particle-in-cell simulation of the laser-driven source. The following sections describe the design of the individual components of LhARA.

This note will be re-issued from time to time to document the parameter set of the current baseline design.

2 Design performance

The performance of LhARA has been evaluated with start-to-end simulations to determine the efficiency and capabilities of the beam transport lines, the dose rates, and the dose distributions at the end stations. The expected maximum dose rates are summarized in **Table 1**. A more detailed description of how the dose rates were evaluated is given in section 6 and in [1].

The particle tracking done as part of the pre-CDR [1] showed that a horizontal and vertical beam width of $\sim$3.5 cm can be achieved in the low-energy *in-vitro* end station with octupoles and collimation for an ideal Gaussian beam at the source. **Figure 1** shows the beam phase space and particle distributions at the Stage 1 end station. An initial verification of the performance of the beam transport line in Stage 1 was done with the use of a 3-D proton distribution at the source sampled from the result of a 2-D particle-in-cell simulation of the laser-target interaction. The dose distribution at the Stage 1 end station obtained with the sampled beam was comparable to the one obtained with the ideal beam. Further verification is required with ion distributions from full 3-D particle-in-cell simulations of the source and with heavier ion species.

In the high-enegy *in-vitro* and *in-vivo* end stations of Stage 2, the almost parallel beam that LhARA will deliver can be varied to illuminate a circular area with a maximum diameter of between 1 and 3 cm with an almost uniform dose, or focused to a spot with diameter of $\sim$1 mm.

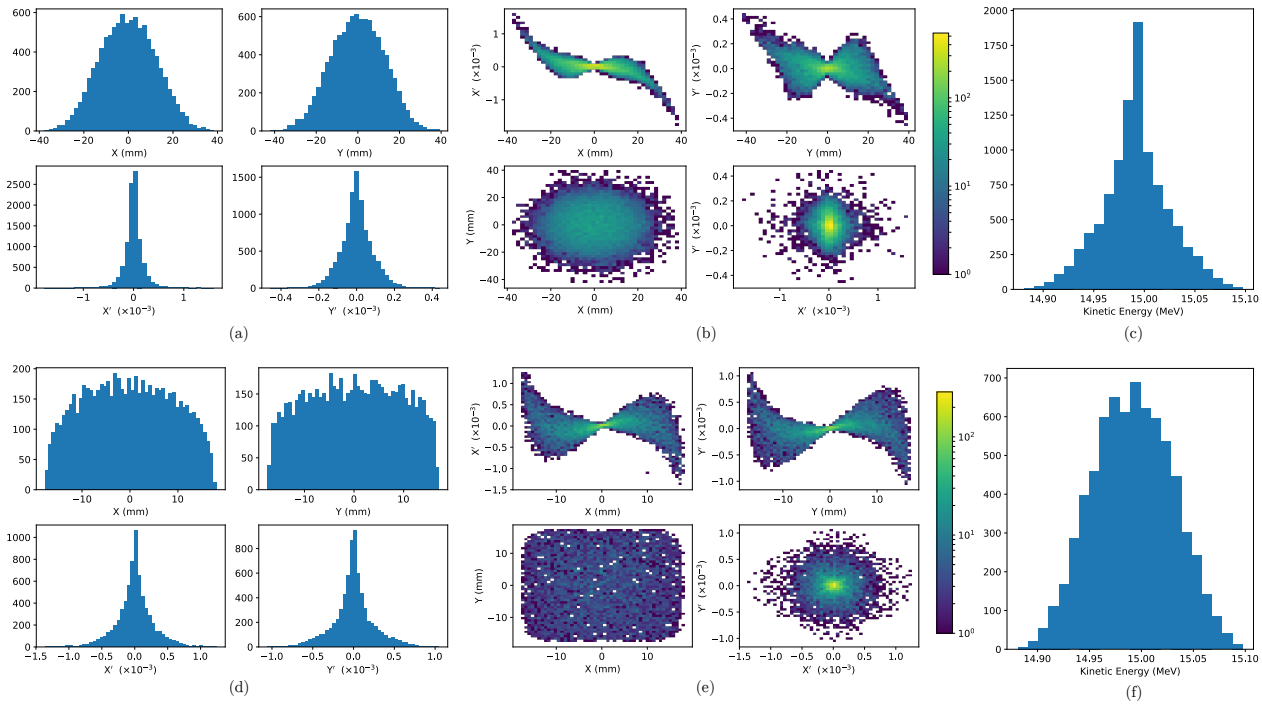

Figure 1: Beam phase space distributions at the end-station in the transverse plane, (X, Y); X′ and Y′ give the slope relative to the Z axis. The transverse phase space is shown in the top two rows for simulations without octupolar focusing and collimation, with the kinetic energy distribution shown in the last column. The same phase space distributions simulated with the effect of octupoles and collimation are shown in the figures in the bottom two rows.

Table 1: Summary of expected maximum dose per pulse and dose rates that LhARA can deliver for minimum beam sizes. These estimates are based on Monte Carlo simulations. The average dose rate is based on the 10 Hz repetition rate of the laser source.

	protons			**carbon**
Kinetic energy	**12 MeV**	**15 MeV**	**127 MeV**	**33.4 MeV/u**
Bunch length	7 ns	7 ns	41.5 ns	75.2 ns
Dose per pulse	7.1 Gy	12.8 Gy	15.6 Gy	73.0 Gy
Instantaneous dose rate	1.0×10^9 Gy/s	1.8×10^9 Gy/s	3.8×10^8 Gy/s	9.7×10^8 Gy/s
Average dose rate	71 Gy/s	128 Gy/s	156 Gy/s	730 Gy/s

3 Ion source

Laser-accelerated ion beams exhibit a quasi-thermal continuous spectrum up to a sharp cut-off maximum energy. To avoid shot-to-shot variations in the flux of particles from the source, the choice has been made to select particles from a region of the energy spectrum of the laser-accelerated bunch well separated from the maximum energy cut-off. To create the flux required in the plateau region, it is proposed to use a commercially available laser that is capable of delivering laser pulses with the parameters specified in **Table 2**. The laser contrast is expected to be better than $10^{10} : 1$ and the shot-to-shot stability better than 1%. The target system must allow operation at 10 Hz in a reproducible manner. For LhARA, a tape drive is proposed that is based on the system developed at Imperial College London. Such tape-drive targets have been shown to be capable of delivering high charge of up to 100 pC at $15\,\mathrm{MeV} \pm 1\,\mathrm{MeV}$ (i.e. $>10^9$ protons per shot).

Proper conditioning of the target, such as cleaning the target surface with a secondary laser to remove contaminant hydrocarbons, allows enhanced acceleration of heavier ions including carbon and oxygen. The evaluation of the performance of LhARA has been done prior to this technical note for proton beams and preliminary C^{6+} beams. Particle-in-cell simulations of the interaction between the laser and the target will allow a more comprehensive evaluation of the beam transport for ion species heavier than the proton.

Table 2: Design parameters of the laser-driven proton and ion source.

Parameter	**Value**	**Unit**
Laser power	100	TW
Laser energy	2.5	J
Laser pulse length	25	fs
Laser rep. rate	10	Hz
Required maximum proton energy	15	MeV

Table 3: Design parameters of the nozzle at the interface between the vacuum vessel of the laser and the vacuum vessel of the first Gabor lens.

Parameter	**Value**	**Unit**
Distance from the target to the entry face	5	cm
Length	5	cm
Entrance aperture radius	2.00	mm
Exit aperture radius	2.87	mm

4 Stage 1 beam transport

The Stage 1 beamline has been designed to minimise the number of times the beam is brought to a focus to reduce the impact of space-charge forces on the beam phase-space. Furthermore, the transport line must produce a uniform dose distribution at the end station and deliver a $\pm 2\%$ energy spread. Beam losses must be minimized for radiation safety and to maximize the dose that can be delivered in a single shot

The proton distribution that leaves the laser-driven source has a large energy spread. In order to reduce the width of the energy spectrum delivered to the low-energy *in-vitro* end station, the protons pass through several collimators. Most of the low-energy particles are absorbed by a conical nozzle at the interface between the vacuum vessel of the laser and the vacuum vessel of the first Gabor lens. The tapering nozzle, which has a smaller entrance aperture compared to the exit aperture, allows different vacuum pressures to be maintained in the target chamber and the vessel of the first lens. The design parameters of the nozzle are listed in **Table 3**. After the nozzle, the beam consists of a continuous spectrum of energies between a few MeV and the maximum energy produced at the target.

The components of the Stage 1 beamline can be grouped according to their role in the transport of the beam: beam capture, matching and energy selection, vertical arc, and an abort line.

Ion capture

The first two Gabor lenses downstream of the source capture the highly divergent proton flux and bring the beam from point to parallel. Two lenses are used instead of one to reduce the maximum plasma density required to focus the beam. **Table 4** specifies the design parameters of the components in the capture section. As an alternative technology to the plasma lenses, normal and superconducting solenoids have been assessed and a preliminary design developed. **Table 4** also includes the required length and maximum field strength of the alternative solenoids. In the event that the solenoid-capture option is selected, a Wien filter will be required to allow the selection of a particular ion species. The design of the Wien filter has yet to be finalised. Downstream of the capture section, an RF cavity permits control of the bunch length and manipulation of the longitudinal phase-space. **Table 4** specifies the radius of the electron plasma required for the full beam to pass through a uniform focusing field. The radius of the electrodes that confine the plasma needs to be determined based on further investigations to limit the formation of instabilities in the plasma.

Table 4: Design parameters of the components of Stage 1 ion-capture section.

Parameter	**Value**	**Unit**
Beam divergence to be captured	50	mrad
Gabor lens effective length	0.857	m
Gabor lens length (end-flange to end-flange)	1.157	m
Gabor lens plasma radius	0.0365	m
Gabor lens maximum voltage	65	kV
Number of Gabor lenses	2	
Alternative technology: solenoid length	1.157	m
Alternative technology: solenoid max field strength	1.3	T

Beam matching and energy selection

The capture section is followed by the components for beam matching and energy selection. A third Gabor lens focuses the beam to a small spot. A collimator at the focus is used to select the beam energy. A second RF cavity is located to allow further manipulation of the longitudinal phase-space. Two further Gabor lenses bring the beam from point to parallel before it enters the vertical $90\,\mathrm{degree}$ arc. **Table 6** specifies the maximum plasma density required to produce the design focusing strength in each of the five Gabor lenses together with the magnetic field strength of the alternative solenoid with an equivalent focal length. Two octupole magnets are placed in the beamline to achieve a uniform beam at the *in-vitro* end station. One octupole is placed after the final Gabor lens where the beam is large and the third order focusing effect of the octupole is more significant. In the beam-tracking simulations of Stage 1, the octupoles were assumed to have a magnetic length of $0.1\,\mathrm{m}$ and pole-tip radius of $5\,\mathrm{cm}$. For an initial evaluation of the effect of the octupoles on the beam distribution at the end station, the strength parameter, k_3, of each octupole was set to 6000. Schemes with similar normalized octupole strengths were designed and demonstrated to produce uniform beams for biomedical research. The strength and the position of the octupoles will be revisited and optimised to maximise the uniformity of the dose at the low-energy *in-vitro* end station.

To further reduce the energy spread of the beam that exits the vacuum nozzle upstream of the first Gabor lens to $\pm 2\%$, three elliptical collimators are placed at key locations along the Stage 1 beamline. The position and the aperture of each collimator are specified in **Table 5**. The first collimator is placed at the location where the nominal energy protons are brought in focus by the third Gabor lens. As the focal length of the Gabor lens is a function of the beam energy, the protons with a large energy deviation from the nominal value are absorbed by the walls of the first collimator significantly reducing the energy spread of the beam. A second beam-shaping collimator is placed at the entrance of the vertical arc to remove protons with large excursion from the ideal trajectory. Finally, a third collimator for momentum cleaning is located at the middle point of the vertical arc in a large dispersion region. The momentum collimator removes the tails of the energy distribution that passes the two upstream collimators. The transmission efficiency of the beam line is $\approx 100\%$ within the $\pm 2\%$ energy interval based on proton tacking simulations without space-charge and with no octupoles. With the inclusion of octupoles and collimation, a total beam width of $3.58\,\mathrm{cm}$ horizontally and $3.46\,\mathrm{cm}$ vertically can be achieved with an associated transport efficiency of $\sim 70\%$. Further optimization is required to improve uniformity whilst optimizing beam-line transmission.

Table 5: Design parameters of the elliptical collimators used for energy and momentum selection in Stage 1 of LhARA.

Element	**Position [m]**	**Horizontal half width [mm]**	**Vertical half width [mm]**
Collimator 1	5.753	1.5	1.5
Collimator 2	10.65	23	23
Collimator 3	12.95	19	6.9

Table 6: Nominal electron plasma density of the five Gabor lenses for beam transport in the Stage 1 of LhARA. The table also specifies the flux density required from a solenoid with an equivalent focusing strength and identical effective length.

Element	**Plasma density [$\mathbf{m^{-3}}$]**	**Magnetic flux density of equivalent solenoid [T]**
Gabor lens 1	5.4×10^{15}	1.4387
Gabor lens 2	7.2×10^{14}	0.5271
Gabor lens 3	1.7×10^{15}	0.8139
Gabor lens 4	1.4×10^{15}	0.7284
Gabor lens 5	1.0×10^{15}	0.6338

Table 7: Design parameters of the components of the Stage 1 sections for matching, energy selection, and beam delivery to low-energy end station.

Parameter	**Value**	**Unit**
Number of Gabor lenses	3	
Number of re–bunching cavities	2	
Number of collimators for energy selection	1	
Arc bending angle	90	Degrees
Number of bending magnets	2	
Number of quadrupoles in the arc	6	
Alternative technology: solenoid length	1.157	m
Alternative technology: solenoid max field strength (to serve the injection line to the Stage 2)	0.8 (1.4)	T

Vertical arc

The vertical arc uses transparent optics in an achromat matching section to ensure that the first-order transfer map through the arc is equivalent to the identity transformation and that any dispersive effects are cancelled. The arc is followed by a $2\,\mathrm{m}$ drift tube to penetrate the concrete shielding and the end-station floor and to bring the beam to bench height. The main design parameters of the beamline components after the beam capture section are specified in **Table 7**.

The last section of the Stage 1 beamline is the abort line. If the first dipole in the vertical arc is ramped down, the beam enters the abort line which consists of a drift space and a beam dump.

5 Post-acceleration (Stage 2)

In LhARA Stage 2, a fixed-field alternating gradient accelerator (FFA), based on the spiral scaling principle, will be used to accelerate the ions to energies higher than those delivered by the laser-driven source. The FFA will increase the momentum of the beam by a factor of three, which will result in a maximum proton-beam energy of $127\,\mathrm{MeV}$ from an injected beam of $15\,\mathrm{MeV}$. For carbon ions (C^{6+}) with the same rigidity, a maximum energy of $\sim 33.4\,\mathrm{MeV/u}$ can be produced.

Injection

The beam energy at the extraction of the FFA will be determined by the energy at injection. Control over the energy at injection into the FFA is obtained by varying the focusing strengths and the RF phases in the Stage 1 beamline. Thus, the required energy slice from the broad spectrum produced at the source is transported to the FFA. This scheme simplifies the injection and extraction systems since their geometry and location can be fixed. The injection line matches the Twiss β functions in both transverse planes and the dispersion of the beam to the values dictated by the periodic conditions in the FFA cell. The presence of dispersion in the injection line allows a collimator to be installed for momentum selection before injection.

A full aperture, fast injection of the beam will be performed using a magnetic septum, installed on the inside of the ring, followed by a kicker magnet situated in a consecutive lattice cell. The specifications of the injection system are dictated by the parameters of the beam at injection, which are summarized for the nominal proton beam in **Table 8**. The beam at injection has a relatively small emittance and short bunch length, which limits the intensity accepted by the ring due to the space-charge effect. An intensity of $\sim 10^9$ protons will be accepted by the ring assuming the nominal beam parameters.

Table 8: Summary of the main parameters for the proton beam at the injection to the FFA ring. These parameters correspond to the nominal (maximum) acceleration mode of operation.

Parameter	**Value**	**Unit**
Beam energy	15	MeV
Total relative energy spread	± 2	%
Nominal physical RMS emittance (both planes)	4.1×10^{-7}	π m rad
Incoherent space charge tune shift	-0.8	
Bunching factor	0.023	
Total bunch length	8.1	ns
Bunch intensity	10^9	

FFA

Table 9 gives the main design parameters of the FFA ring. The ring consists of ten symmetric cells, each containing a single combined-function spiral magnet. The choice of the number of cells is a compromise between the size of the orbit excursion, which dictates the radial extent of the magnet, and the length of the straight sections required to accommodate the injection and extraction systems. The magnet gap of $4.7\,\mathrm{cm}$ given in **Table 9** is estimated assuming a flat-pole design for the FFA magnets.

The acceleration of the beam will be done using an RF system operating at harmonic number $h = 1$ with an RF frequency in the range from 2.89 to $6.48\,\mathrm{MHz}$. The RF voltage required for 10 Hz operation is $0.5\,\mathrm{kV}$. However, at this relatively low voltage the energy acceptance at injection is $\pm 0.7\%$. Operating with a voltage of $4\,\mathrm{kV}$ increases the energy acceptance to $\pm 2\%$. This voltage can be achieved with one cavity. Here, two cavities are proposed to provide greater operational stability.

Extraction and transport to the end stations

Substantial margins in the beam parameters were assumed in the design of the extraction line from the FFA due to uncertainties in the beam distributions originating from the Stage 1 beam transport, the FFA injection line, and potential distortions introduced by the presence of space-charge effects during acceleration in the ring. The beam emittance was therefore allowed to be as large as a factor of 10 greater than the nominal value, which was derived by assuming that the normalized emittance is conserved from the source, through the Stage 1 beam line, and in the FFA ring. In the nominal case, the physical emittance of the beam is affected by adiabatic damping only. Substantial flexibility in the optics of the extraction line is required, as the extraction line must accommodate a wide spectrum of beam conditions to serve the *in-vitro* and *in-vivo* end-stations. Detailed

Table 9: Design parameters of the components of the Stage 2 beam transport: transfer lines and the FFA.

Parameter	Value or range	Unit
Injection line		
Number of bending magnets in the injection line	7	
Number of quadrupoles in the injection line	10	
FFA		
FFA: Machine type	single spiral scaling FFA	
FFA: Extraction energy	15–127	MeV
FFA: Number of cells	10	
FFA: Orbit $R_{\min}$	2.92	m
FFA: Orbit $R_{\max}$	3.48	m
FFA: Orbit excursion	0.56	m
FFA: External R	4	m
FFA: Number of RF cavities	2	
FFA: RF frequency	1.46–6.48	MHz
FFA: harmonic number	1, 2 or 4	
FFA: RF voltage (for 2 cavities)	4	kV
FFA: spiral angle	48.7	Degrees
FFA: Max B field	1.4	T
FFA: k	5.33	
FFA: Magnet packing factor	0.34	
FFA: Magnet opening angle	12.24	Degrees
FFA: Magnet gap	0.047	m
FFA: Ring tune (x,y)	(2.83,1.22)	
FFA: γ_T	2.516	
FFA: Number of kickers	2	
FFA: Number of septa	2	
Extraction line		
Number of bending magnets in the extraction line	2	
Number of quadrupoles in the extraction line	8	
Vertical arc bending angle	90	Degrees
Number of bending magnets in the vertical arc	2	
Number of quadrupoles in the vertical arc	6	
Number of cavities for longitudinal phase space manipulation	5	
Number of quadrupoles in the in vivo beam line	4	

Table 10: Comparison of magnet parameters in the vertical arc between Stage 1 and Stage 2 of LhARA. The quadrupole in the arc with the highest strength was reported in both cases which would require the highest magnetic field.

Parameter	**Stage 1 arc**	**Stage 2 arc**
Maximum energy (proton)	15 MeV	127 MeV
Maximum beam radius	5 cm	5 cm
Dipole bend angle	$\pi/4$	$\pi/4$
Dipole bend length	0.8 m	1.2 m
Quadrupole maximum strength	3.15 m^{-2}	2.74 m^{-2}
Quadrupole length	0.1 m	0.3 m

studies were carried out for proton beams with kinetic energies of 40 and $127\,\mathrm{MeV}$. **Table 11** gives the Twiss β values for different beam sizes for the 40 and $127\,\mathrm{MeV}$ proton beam energies assuming a Gaussian beam distribution. The optics and geometric acceptance of the system is approximately the same for the 40 and $127\,\mathrm{MeV}$ beams, justifying the working hypothesis that beam emittance is approximately the same for both beam energies. This assumption will be revised as soon as space-charge simulations for the entire system are available.

The first two dipoles and four quadrupoles of the extraction line bend the beam coming from the extraction septum of the FFA such that it is parallel to the low-energy beam line while ensuring that dispersion is closed. Closing the dispersion is critical, as off-momentum particles will follow trajectories different to those followed by particles with the design momentum and therefore impact the size and shape of the beam downstream. The second part of the extraction line consists of four quadrupoles which transport the beam either to the first dipole of the vertical arc or to the transport line leading to the *in-vivo* end station.

The FFA is followed by a 90° vertical arc to send the beam to the high energy *in-vitro* end station. If the first dipole in the arc is not energised, the beam will be sent to the *in-vivo* end station. An additional switching dipole located in the extraction line can be energized to send the beam to the high-energy beam dump. The detailed design of the high-energy abort line will have to ensure that no stray radiation enters the end stations.

The 90° vertical bend is a scaled version of the low-energy vertical arc, following the same design principles, and consists of two bending dipole magnets and six quadrupole magnets. To accommodate the higher beam energies, the lengths of the magnets were scaled in order to ensure that peak magnetic fields were below the saturation limits of normal conducting magnets. A comparison of the Stage 2 arc with the Stage 1 arc is presented in **Table 10**. The dipole bending magnets have the bend length increased from $0.8\,\mathrm{m}$ to $1.2\,\mathrm{m}$. The quadrupole magnet lengths were tripled from $0.1\,\mathrm{m}$ to $0.3\,\mathrm{m}$. Scaling the magnet lengths increases the arc length from $4.6\,\mathrm{m}$ to $6\,\mathrm{m}$, which means the Stage 2 arc ends about $0.9\,\mathrm{m}$ higher compared to that of Stage 1. To compensate for this, the final drift length in the Stage 1 beam line was lengthened to ensure both arcs end at the same height.

To facilitate efficient small-animal handling, the end station dedicated to *in-vivo* experiments will be positioned adjacent to the principle road access to the facility. If the first dipole of the high-energy *in-vitro* arc is not energized, the beam is sent to the *in-vivo* end station. From the end of the extraction line, $7.7\,\mathrm{m}$ of drift is necessary to clear the first bending dipole of the *in vitro* arc, to provide space for the five RF cavities needed for longitudinal phase-space manipulation and to allow space for diagnostic devices. Following this drift is a further $6.6\,\mathrm{m}$ of beam line that includes four quadrupoles, each of length $0.4\,\mathrm{m}$, which are used to perform the

Table 11: Beam emittance values and target β values for different beam sizes for 40 MeV and 127 MeV beams. The beam size is taken to be four times the sigma of the transverse beam distribution.

	40 MeV protons (Nominal)	**127 MeV protons (Nominal)**	**127 MeV protons (Pessimistic)**
RMS Emittance (ϵ_x, ϵ_y) [π mm mrad]	0.137	0.137	1.37
β [m] for a 1 mm spot size	0.46	0.46	0.039
β [m] for a 10 mm spot size	46	46	4.5
β [m] for a 30 mm spot size	410	410	40

final focusing adjustments of the beam delivered to the *in-vivo* end station. A final $1.5\,\mathrm{m}$ drift length is reserved for scanning magnets so spot scanning can be performed and to allow for penetration of the shielding of the *in-vivo* end station. In total, the *in-vivo* beam line is $15.6\,\mathrm{m}$ in length. The flexible design can match the various $\beta_{x,y}$ values given in **Table 11**, but not the smallest target value of $\beta_{x,y} = 0.039\,\mathrm{m}$ for the pessimistic scenario, which is very challenging.

6 End stations

The maximum dose that can be delivered was evaluated for a variety of beam energies and is summarised in **Table 1**. In order for the dose to be reported in units of Gray it is necessary to define the volume within which the energy deposition is to be integrated. Therefore, the dose was estimated from simulations by calculating the energy deposited in a volume of water corresponding in size to the sensitive volume of a PTW 23343 Markus ion chamber placed at the position of the Bragg peak. This choice allows the doses and dose-rates reported here to be compared to those of operating facilities. The cylindrical sensitive volume of the ion chamber has a radius of $2.65\,\mathrm{mm}$ and a depth of $2\,\mathrm{mm}$, giving a volume of about $4.4 \times 10^{-8}\,\mathrm{m}^3$. The total energy deposited within the chamber was recorded and converted into dose in units of Gray.

For the high-energy *in-vitro* end station, a similar design to the low-energy end station was used, but the air gap was increased from 5 mm to 5 cm and a water phantom was placed at the end of the air gap instead of a cell culture plate. The water phantom used in the simulation was based upon the PTC T41023 water phantom. The end-station design assumed for a 33.4 MeV/u carbon beam was the same as that used for the low-energy *in-vitro* end station due to the limited range in water of the carbon beam. . The intensity of the beam is assumed to be a factor of 12 less than that for protons in order to preserve the same strength of the space-charge effect at injection into the FFA with the same beam parameters because the incoherent space charge tune shift is proportional to q^2/A and inversely proportional to $\beta^2\gamma^3$, where q is the particle charge, A its mass number, and β and γ its relativistic parameters.

Additional parameters used in the design of the end stations are listed in **Table 12**.

Table 12: Design parameters of the components of the *in vitro* and *in vivo* end stations.

Parameter	Value or range	Unit
***In vitro* biological end stations**		
Maximum input beam diameter	1–3	cm
Beam energy spread (full width)	Low-energy end station: ≤ 4	%
	High-energy end station: ≤ 1	%
Input beam uniformity	< 5	%
Scintillating fibre layer thickness	0.25	mm
Air gap length	5	mm
Cell culture plate thickness	1.3	mm
Cell layer thickness	0.03	mm
Number of end stations	2	
***In vivo* biological end station**		
Maximum input beam diameter	1–3	cm
Beam energy spread (full width)	≤ 1	%
Input beam uniformity	< 5	%
Beam options	Spot-scanning, passive scattering, micro-beam	

References

[1] G. Aymar, T. Becker, S. Boogert, M. Borghesi, R. Bingham, C. Brenner, P. N. Burrows, O. C. Ettlinger, T. Dascalu, S. Gibson, T. Greenshaw, S. Gruber, D. Gujral, C. Hardiman, J. Hughes, W. G. Jones, K. Kirkby, A. Kurup, J.-B. Lagrange, K. Long, W. Luk, J. Matheson, P. McKenna, R. McLauchlan, Z. Najmudin, H. T. Lau, J. L. Parsons, J. Pasternak, J. Pozimski, K. Prise, M. Puchalska, P. Ratoff, G. Schettino, W. Shields, S. Smith, J. Thomason, S. Towe, P. Weightman, C. Whyte, and R. Xiao, "LhARA: The Laser-hybrid Accelerator for Radiobiological Applications," *Frontiers in Physics* **8** (2020).